

Lab on a Chip

Accepted Manuscript



This is an *Accepted Manuscript*, which has been through the Royal Society of Chemistry peer review process and has been accepted for publication.

Accepted Manuscripts are published online shortly after acceptance, before technical editing, formatting and proof reading. Using this free service, authors can make their results available to the community, in citable form, before we publish the edited article. We will replace this *Accepted Manuscript* with the edited and formatted *Advance Article* as soon as it is available.

You can find more information about *Accepted Manuscripts* in the [Information for Authors](#).

Please note that technical editing may introduce minor changes to the text and/or graphics, which may alter content. The journal's standard [Terms & Conditions](#) and the [Ethical guidelines](#) still apply. In no event shall the Royal Society of Chemistry be held responsible for any errors or omissions in this *Accepted Manuscript* or any consequences arising from the use of any information it contains.

Cite this: DOI: 10.1039/c0xx00000x

www.rsc.org/xxxxxx

ARTICLE TYPE

Improved electrochemical detection of transthyretin synthetic peptide in the nanomolar range with a two-electrode system integrated in a glass/PDMS microchip

Mathilde Faure,^{a,b} Antoine Pallandre,^{c,d} Syrine Chebil,^{a,b} Isabelle Le Potier,^{c,d} Myriam Taverna,^{c,d}
Bernard Tribollet,^{a,b} Claude Deslouis,^{a,b} Anne-Marie Haghiri-Gosnet,^e and Jean Gamby^{a,b*}

Received (in XXX, XXX) Xth XXXXXXXXX 20XX, Accepted Xth XXXXXXXXX 20XX

DOI: 10.1039/b000000x

An alternative of three-electrode set-up for electrochemical detection and analysis in microfluidic chips is described here. The design of the electrochemical sensor consists in the surfacing of glass substrate covered by PDMS block which bears the microfluidic channels. A band microelectrode as working electrode surrounded by a large counter electrode is obtained at the micrometric level to propose a simple and efficient sensing area for on-a-chip analysis. The counter-electrode with a surface area about 22-fold greater than the working-microelectrode can also be considered as a pseudo reference since its current density is low and thus limits the potential variations around the rest potential. To this purpose, [Fe(III)(CN)₆]³⁻ / [Fe(II)(CN)₆]⁴⁻ redox couple was used in order to set a reference potential at 0 V since both electrodes are in platinum. The electrochemical microchip performance was characterized using difference pulse voltammetric detection (DPV) and quantification of the optically multi-labelled transthyretin synthetic peptide mimicking a tryptic fragment of interest for the diagnosis of familial transthyretin amyloidosis (ATTR). The limit of detection at working microelectrode for peptide was 25 nM, a value 100-fold lower than the one reported with conventional capillary electrophoresis coupled with laser-induced fluorescence under the same analytical conditions.

1 Introduction

Over the past two decades, laser-induced fluorescence (LIF)^{[1],[2],[3],[4]} and mass spectrometry (MS)^{[5],[6],[7],[8]} coupled with microchip have benefited from a considerable growth because of their potentiality for proteomic analysis. Although LIF and MS offer high sensitivity and powerful information, they require large and bulky instrumentation significantly impairing the portability of such instruments. In contrast, the development and availability of microsized electrodes for electrical detection in microfluidic chips have been delayed with respect to the improvement of the technology development of μ TAS.^{[5],[9],[10],[11],[12],[13]} For this challenge, electrochemical techniques are more suitable for the detection of ionic species (oxidable or reducible) because they have the unique advantage to convert chemical or electrochemical events into electrical signal response. The relevance of electrochemical detection in flow-channel microelectrode with the improvement of electrode size fabrication has been widely proven, including the use of amperometric or voltammetric detections while hydrodynamics of the streaming electrolyte solution was controlled.^{[14],[15],[16]} According to the microchip dimensions such as the size ratios and geometries electrode/channel, a steady-state current is reached that is ascribed to mass transport limitation.^{[14],[17],[18],[19]} This latter can be measured with precision assuming that electron transfer at the

working microelectrode is fast enough. Briefly, the advantages for the use of flow-channel microelectrodes include: measurements on very small volumes and low quantity of biological sample, the ohmic drop of potential decreases since the recorded current is low and the improvement of the ratio between faradaic and charging current since this latter is related to the electrode surface area and also because the signal/ noise ratio of the electrogenerated species has a strong impact on the detection limit. Nevertheless, accurate measurements of electrochemical potentials in microchip are most often required to be properly controlled using a three-electrode set-up which includes a reference electrode. Aside from the efficiency in terms of sensitivity obtained with this configuration, repeatability and reproducibility of results in microchip remain difficult to reach. These limitations are due to difficulties encountered to make a stable reference electrode over time in miniaturized devices. Indeed, interferences on the measured signal may occur. For instances parasitic processes at the reference electrode surface (passivation, adsorption, bubble generation, dissolution...) interfere with the signal of interest. Some restrictions were alleviated by the use of thin-film Ag/AgCl microelectrodes compatible with microfluidics for separation and detection in microchips.^{[20],[21]} However, the remaining problem with Ag/AgCl as reference is its poor stability over time which is attributed to partially or totally dissolution of the thin layer

leading to mixed potentials.

Since the two-electrode set-up has been used in interdigitated microelectrodes array strategy for nucleic acids screening^{[22],[23]} or in technological conception of DNA biosensors,^[24] this paper presents a strategy consisting to network a flow-channel with a band microelectrode as working electrode surrounded by a millimetric electrode as counter-electrode. The counter-electrode with a surface area about 22-fold greater than that of the working microelectrode can be considered as a pseudo reference since its current density variation is low in comparison to the one of the working microelectrode. This aim is reached by the use of $[\text{Fe(III)(CN)}_6]^{3-} / [\text{Fe(II)(CN)}_6]^{4-}$ redox couple in flow-channel microelectrode during the labelling and detection steps in order to set an equilibrium potential at 0 V as both microelectrodes are in platinum (Figures 1A-C).

The fluidic microdevice with two-microelectrode set-up was validated by using a previously well-tested differential pulse voltammetric (DPV) detection protocol of multi-labelled synthetic peptide (PN) of interest in the diagnosis of familial transthyretin amyloidosis (ATTR).^[25] The dimensions (channel width and height) of the PDMS microchannel indicated in Figure 1C have been selected in order to establish a laminar flow and designed using soft fabrication technique, while hard fabrication techniques have been used for integrating several pairs of two electrodes networks in the same microchannel for multi-detection purposes (Figure 1B-C).

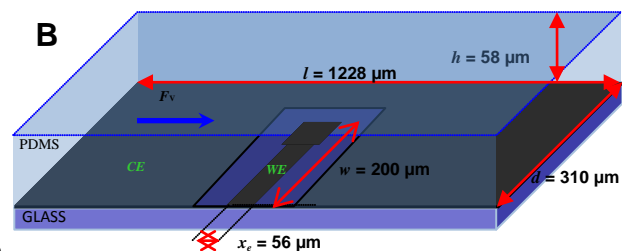
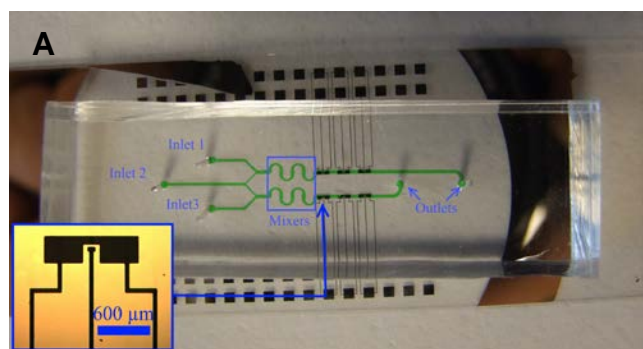


Figure 1 A. Picture of several pairs of two microelectrodes networks located on the microchannel junction for multi-detection possibility. The fluidic microchannels allowing the sample injection with several configurations (inlet 1, 2, 3). B. Schematic view of the detection area with a pair of microelectrodes (CE: counter electrode, WE: working electrode). The fluidic channel, WE and CE microband electrodes characteristic dimensions: h , d , w , x_c and l are indicated and the B scheme is not to the scale.

2 Materials and methods

2.1 Chemicals

Naphtalene-2,3-dicarboxyaldehyde (NDA), potassium cyanide and boric acid were purchased from Sigma-Aldrich (Saint-Quentin Fallavier, France). Methanol and sodium hydroxide were obtained from VWR (Fontenay-sous-Bois, France). The 22-aa synthetic peptide (PN) (N-term TSESGELHGLTTEEEFVEGIYK C-term) mimicking a tryptic fragment of interest for the diagnosis of ATTR was obtained from Genepep (Prades-le-Lez, France).

2.2 Peptide labelling conditions

PN was covalently labelled with NDA, an amine-reactive dye with fluorogenic and electroactive properties. The protocol of the labelling reaction was previously optimized and published elsewhere using both capillary electrophoresis coupled with laser-induced fluorescence detection (CE-LIF)^{[26],[27]} and DPV detection.^[25] In brief, optimal conditions for DPV detection were obtained when $[\text{NDA}]_{\text{total}} / [\text{amino acid or peptide}] = 100$ and $[\text{NDA}]_{\text{total}} / [\text{CN}^-] \text{ ratio} = 1$ with an incubation time of 15 min in 100 mM borate buffer pH 9 at room temperature. DPV experiments were carried out in traditional three-electrode cell to characterize NDA-labelled PN with a glassy carbon electrode as WE. These experiments highlighted that the labelled PN could be detected at low concentration (LOD = 5 μM). The oxidation peaks for the N-2-substituted-1-cyanobenz- $[\beta]$ -isoindole derivative (CBI) have been observed at 0.55-0.7 V/SCE. DPV experiments showed also that the two NH_2 groups of PN (aliphatic ϵ - NH_2 of C-term Lys and N-term Thr) can be tagged to form both di-tagged and mono derivatives (CBI-TSESGELHGLTTEEEFVEGIYK-CBI), which were detected at 0.55 V/SCE and 0.69 V/SCE, respectively.^[25]

2.3 Microchip Network

The designs of the lithographic masks have been done with the L-Edit software (from Tanner EDA). To fabricate the microchip we used two masks, one to surface the fluidic microchannels and the second one for the electrodes. Both masks have been first printed on a plastic slide at high resolution (selba Switzerland). All lithographies have been carried out with a Karl Suss manual mask aligner MJB3 (Süss Microtec). To increase the reproducibility of the two lithographic steps, we transferred the patterns of the plastic mask onto glass wafer bearing a 150 nm layer of chromium. An inverted lithography by UV irradiation of AZ5214 (from MicroChemicals, Germany) has been done prior to a chrome etch to build the chromium master masks. All substrates were always cleaned with piranha solution (50/50 v/v of $\text{H}_2\text{SO}_4/\text{H}_2\text{O}_2$ - caution this solution may lead to exothermic reaction with projections) for 20 min and then abundantly rinsed with deionised water. The 500 μm thick borosilicate glass rectangular slides (from Opticad, France) have been cleaned and spin-coated with AZ5214 to pattern the electrodes and the electrical junctions with square contact with a 5 \AA thick layer of titanium and 250 \AA of platinum by a classic lift-off process. The fluidic network is obtained from a master mold made with SU-8. The fabrication of this master mold is started with the cleaning of the silicon wafer and lithography of a 16 μm thick layer of SU-8.

A 1 cm thick layer of PDMS is poured onto the SU-8 master mold to get a negative replica after overnight curing at 70°C of the fluidic network. The PDMS and the glass substrates with the electrodes are washed with isopropanol and dried with nitrogen. Then the PDMS part is treated with nitrogen plasma to favour the adhesion of the PDMS onto the glass slide. The manual alignment of the PDMS and electrodes is done under binocular for the correct positioning of the electrodes in the microfluidic chips.

2.4 Apparatus

Electrochemical measurements were performed by using a Biologic SP-300 electrochemical analysis system with EC-lab software. Experiments were performed with a two-electrode cell configuration. The counter-electrode and the working electrode were both in platinum (Pt) with areas equal to $30.57 \times 10^{-4} \text{ cm}^2$ and $1.38 \times 10^{-4} \text{ cm}^2$, respectively. The scan rate used for cyclic voltammetry experiments was varied from $1 \text{ mV} \cdot \text{s}^{-1}$ to $100 \text{ mV} \cdot \text{s}^{-1}$. Differential pulse voltammetry parameters as modulation time (100 ms), modulation amplitude (7.5 mV) and scan rate ($25 \text{ mV} \cdot \text{s}^{-1}$) have been optimized to obtain well-defined analytical curves. These latter were all corrected by eliminating the DPV background response that is recorded on a blank solution.

3. Results and discussion

3.1 Hydrodynamic conditions in flow-channel microelectrode

Hydrodynamic voltammetry in flow-channel electrode was introduced by Compton *et al.* [14]. Indeed, the use of a rectangular channel comprising a microband electrode under laminar flow conditions allows to achieve a mass-transport limited current flowing at the electrode (see Figure 1C). The parameters to be optimized are then: the scan rate and the flow rate in flow-channel electrode. Experimentally, the flow rate imposed by the syringe pump leads to a forced axial convection. The work of Levich [28] had predicted this behaviour in the case of a channel electrode type where intensity of the transport limited current was expressed as follows in equation 1 obtained from the only axial convection and normal diffusion to the electrode:

$$I_{\text{lim}} = 0.925nFC x_e^{2/3} wD^{2/3} \left(4 \frac{F_v}{h^2 d} \right)^{1/3} \quad (1)$$

with: n , the number of electrons exchanged, F , the Faraday constant (96485 C), F_v , the volumetric flow (in $\text{cm}^3 \cdot \text{s}^{-1}$), C , the concentration of electroactive species ($\text{mol} \cdot \text{cm}^{-3}$) and D the diffusion coefficient of the electroactive species ($\text{cm}^2 \cdot \text{s}^{-1}$); x_e , w , h and d , values of dimensions (in μm), are indicated in Figure 1C.

Based on this theoretical relationship, experiments were carried out in our designed two-microelectrode device by adding an equimolar solution of $2 \text{ mM} [\text{Fe(III)(CN)}_6]^{3-} / [\text{Fe(II)(CN)}_6]^{4-}$ redox couple in 0.1 M KCl pumped under laminar flow. Initially, the scan rate was optimized for steady-state current response. For that, a low flow rate of $0.05 \mu\text{L} \cdot \text{s}^{-1}$ was used while scan rate was varied from 1 to $100 \text{ mV} \cdot \text{s}^{-1}$. The obtained voltammograms show

current plateaus for scan rates below $25 \text{ mV} \cdot \text{s}^{-1}$ (Figure 2A). This well-known voltammogram shape was observed as the diffusion mode at the working microelectrode is in quasi steady-state, whereas most typical cyclic voltammograms shape were observed with the presence of an oxidation peak and a reduction peak from $25 \text{ mV} \cdot \text{s}^{-1}$ to $100 \text{ mV} \cdot \text{s}^{-1}$ (Figure 2A). This transition is due to the passage from quasi-steady state to a planar diffusion. As expected, the obtained current intensity response was scan rate dependent because the forced convection controls the shape geometry of the adjacent diffusion layer on microelectrodes. [14],[18],[19],[29],[30]

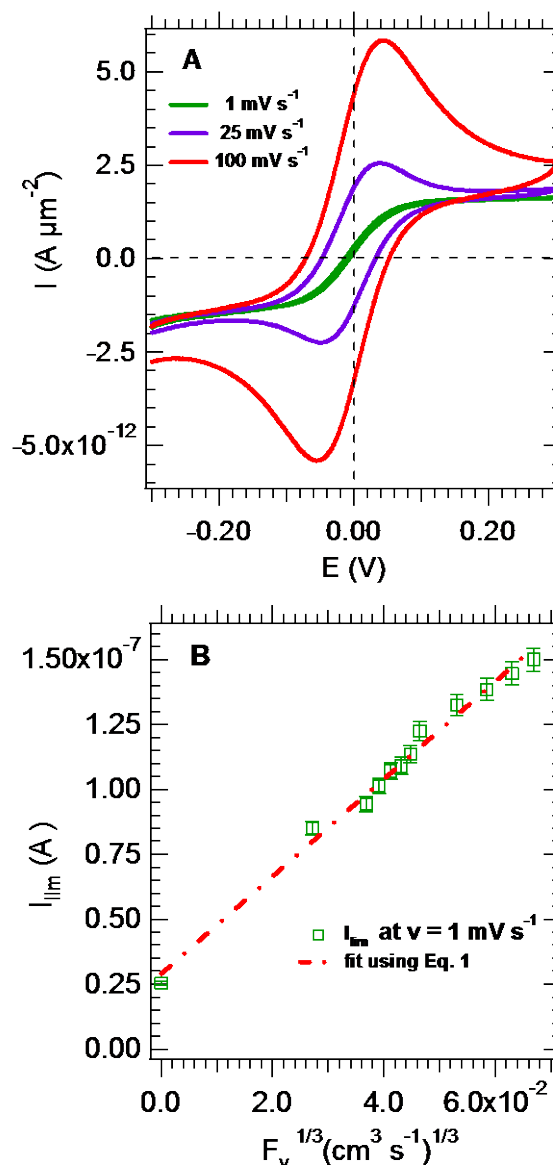


Figure 2. A. Scan rate dependence of the cyclic voltammetric response of WE microband electrode in the described flow channel (see Figure 1C) using $0.05 \mu\text{L} \cdot \text{s}^{-1}$ as fixed value of flow rate (only three scan rates 1, 25 and $100 \text{ mV} \cdot \text{s}^{-1}$ are displayed) with an equimolar solution of $2 \text{ mM} [\text{Fe(III)(CN)}_6]^{3-} / [\text{Fe(II)(CN)}_6]^{4-}$ in 0.1 M KCl . B. Volumetric flow dependence of the transport limited current measured at WE microelectrode using $1 \text{ mV} \cdot \text{s}^{-1}$ as fixed scan rate (where quasi steady-state voltammograms are reached) in the same solution composition.

Squares: experimental values on plateaus. Dotted line: fit using Levich plot (Equation 1 in the text).

In the following experiments, the selected $1 \text{ mV}\cdot\text{s}^{-1}$ scan rate was fixed leading to quasi identical forward and backward waves (6 mV maximum gap). Then, the current plateau variation was measured with flow rates which vary from $0.02 \mu\text{L}\cdot\text{s}^{-1}$ to $0.3 \mu\text{L}\cdot\text{s}^{-1}$. As displayed in Figure 2B, current plateau variation according to the volumetric flow to the power $1/3$ was in agreement with the Levich plot behaviour (Equation 1) using a linear fit equation: $J_{\text{lim}} = 2.89 \times 10^{-8} + 1.88 \times 10^{-6} F_v^{1/3}$ with a good correlation coefficient ($R = 0.994$).

3.2 Difference pulse voltammetric PN peptide detection into microchip in presence of redox couple as reference

The flow rate was also optimized for the DPV experiments for which the optimum flow rate at $0.05 \mu\text{L}\cdot\text{s}^{-1}$ was found suitable for the detection step in the presence of the redox couple. Two different ratios $[\text{Fe(III)(CN)}_6]^{3-} / [\text{Fe(II)(CN)}_6]^{4-}$ were used: a ratio of 1 (ferricyanide and ferrocyanide in equimolar amounts) and 0.25 (0.125 mM ferricyanide and 0.5 mM ferrocyanide concentration in excess). The Nernst equation as follows in equation 2 can be used to predict the Nernst equilibrium potential for the redox couple, E_{eq} .

$$E_{\text{eq}} = E^0_{\text{Fe(CN)}_6^{3-}/\text{Fe(CN)}_6^{4-}} + 0.059 \log \left(\frac{[\text{Fe(CN)}_6^{3-}]}{[\text{Fe(CN)}_6^{4-}]} \right) \quad (2)$$

Indeed, the potential of $[\text{Fe(III)(CN)}_6]^{3-} / [\text{Fe(II)(CN)}_6]^{4-}$ redox couple is expected at 0 V for a ratio of 1, while it must be located at -0.036 V when the ratio is 0.25. Figure 3 shows the oxidation peaks obtained for the DPV detection with the labelled peptide PN-CBI in the presence of both $[\text{Fe(III)(CN)}_6]^{3-} / [\text{Fe(II)(CN)}_6]^{4-}$ ratios. The PN-CBI peak characteristic is observed at 0.4 V with the both ratios while reference peak of ferrocyanide has been shifted to the negative potential of 0.034 V when the 0.25 ratio was used (see Figure 3 and Table 1). The values for the peaks potential are close to the expected values which were estimated using the Nernst equation.

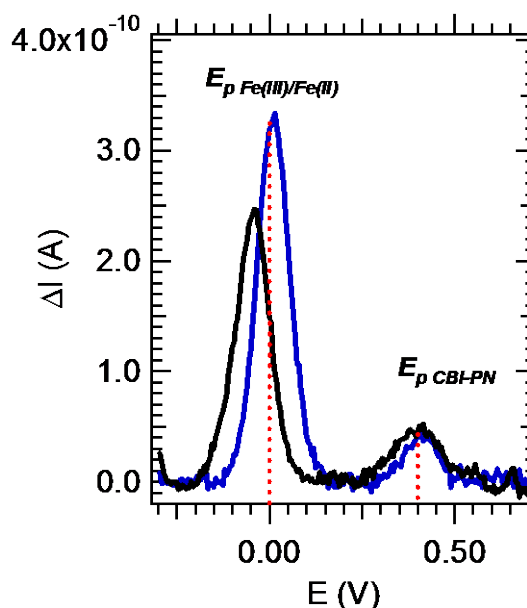


Figure 3. DPV of the peptide labelling with $2.5 \text{ mM NDA } 25 \mu\text{M PN}$ (molar ratio 100), $\text{NDA} / \text{KCN} = 1$ and the presence $[\text{Fe(III)(CN)}_6]^{3-} / [\text{Fe(II)(CN)}_6]^{4-}$ redox couple as potential reference in buffer $100 \text{ mM borate pH } 9 / \text{MeOH (50/50 v/v)}$. Blue curve with $0.125 \text{ mM } [\text{Fe(III)(CN)}_6]^{3-} / 0.125 \text{ mM } [\text{Fe(II)(CN)}_6]^{4-}$ molar ratio 1 and black curve $0.125 \text{ mM } [\text{Fe(III)(CN)}_6]^{3-} / 0.5 \text{ mM } [\text{Fe(II)(CN)}_6]^{4-}$ molar ratio 0.25. Scan rate $25 \text{ mV}\cdot\text{s}^{-1}$ modulation time 100 ms modulation amplitude 7.5 mV under a flow rate of $0.05 \mu\text{L}\cdot\text{s}^{-1}$.

The detection of the labelled peptide was carried out three times for each $[\text{Fe(III)(CN)}_6]^{3-} / [\text{Fe(II)(CN)}_6]^{4-}$ ratio. The peak intensity of the PN-CBI with the two ratios was found at $(4.5 \pm 0.5) \times 10^{-11} \text{ A}$. The values are listed in Table 1 for the oxidation potential peaks with means and standard deviations calculated with three experiments.

Table 1. Values of oxidation peak potential and potential difference between $E_{\text{p PN-CBI}}$ and $E_{\text{p Fe(III)/Fe(II)}}$ according to the used ratio, *i. e.* with $0.125 \text{ mM } [\text{Fe(III)(CN)}_6]^{3-} / 0.125 \text{ mM } [\text{Fe(II)(CN)}_6]^{4-}$ molar ratio 1 and $0.125 \text{ mM } [\text{Fe(III)(CN)}_6]^{3-} / 0.5 \text{ mM } [\text{Fe(II)(CN)}_6]^{4-}$ molar ratio 0.25.

ratio	#	$E_{\text{p PN-CBI}}$ (V)	$E_{\text{p Fe(III)/Fe(II)}}$ (V)	ΔE_{p} (V)
1	1	0.414	0.009	0.405
	2	0.408	0.008	0.4
	3	0.413	0.012	0.401
	mean	0.412 ± 0.003	0.009 ± 0.004	0.402 ± 0.003
0.25	1	0.414	-0.039	0.456
	2	0.396	-0.021	0.417
	3	0.419	-0.043	0.462
	mean	0.415 ± 0.02	-0.034 ± 0.01	0.44 ± 0.03

The obtained peak potential difference is equal to average values of $(440 \pm 30) \text{ mV}$ and $(402 \pm 3) \text{ mV}$ when ratio 0.25 and 1 was used, respectively. Although ratio 1 leads to least standard deviation on peak potential position, the non equimolar ratio can

be viewed as an advantage in some cases, for instance, where a high peak difference is sought for a better separation and therefore a higher peak resolution between reference and analyte. This results confirm that the detection scheme in flow-channel with two microelectrode set-up using redox couple as reference is equally suited than three microelectrodes set-up. Thereafter the methodology with non equimolar ratio will be maintained and optimized in the next experiments.

The detection limit was sought in the microfluidic device by maintaining the NDA / PN and NDA / KCN ratios constant. The experiments were repeated three times for each PN concentration. The microchannel was washed between each detection step by rinsing with deionized water and a reference curve (only Fe(III) / Fe(II)) was made to check the measurement reproducibility. The composition of the peptide samples is shown in Table S1 (see supplementary material). Briefly, for low concentrations of PN, [Fe(III)(CN)₆]³⁻ and [Fe(II)(CN)₆]⁴⁻ concentrations were decreased to better observe the peak of the di-labelled PN. This permits to enhance peak intensity of the di-labelled peptide in comparison to ferrocyanide peak reference. The obtained PN-CBI peak intensity was plotted against PN concentration added in the sample preparation (Figure 4). It has been also observed that the obtained PN-CBI peak intensity corresponding to low concentrations were overestimated as the PN concentration decreases in samples. Indeed, the peaks become broader as previously observed in macrosystem with DPV detection.^[25] This behaviour was attributed to the mono-labelled peak PN-CBI oxidation which has the effect of increasing the intensity of the global peak intensity. A deconvolution fit is displayed in Figure 5 for 0.1 μM PN added. The peaks obtained were then deconvoluted into two DPV peaks located at 0.38 V and 0.5 V corresponding to the di- and mono-labelled peptide detection, respectively. This observation is in accordance to previous experiments with mass spectrometry and separating techniques. The labelling reaction has been extensively characterized as shown in previous paper.^{[25],[27]}

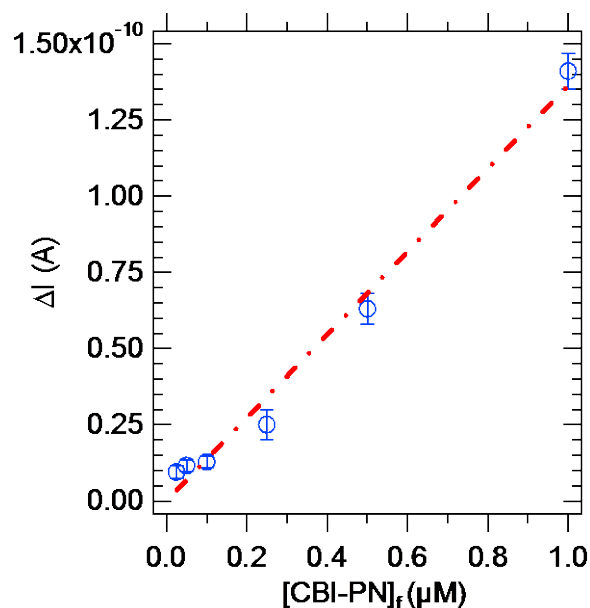


Figure 4. Calibration curve for PN-CBI detection using DPV in the flow-channel microelectrode device. Circles: experimental current intensity around 0.4 V for each experimental DPV at various concentrations from 1 μM to 25 nM (see supplementary material for samples preparation and ratios). The first three points were corrected using peak global deconvolution according to Figure 5. The linear fit: regression coefficient = 0.99, slope = 1.36×10^{-10} A μM⁻¹ (sensitivity).

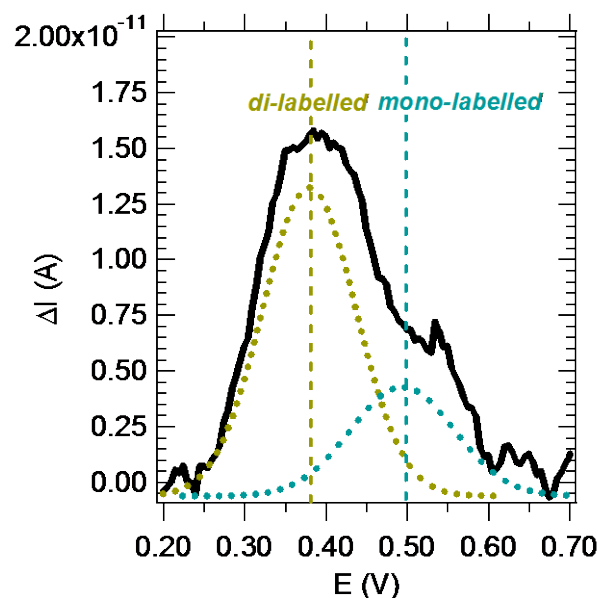


Figure 5. Peak intensity deconvolution at low concentration level (0.1 μM PN total concentration in sample) highlighting the interference of the mono-labelled detection (0.5 V) on enlargement peak obtention (0.38 V). DPV of the di- (gold) and mono- (cyan) labelled peptide detection using 0.01 mM NDA / 0.1 μM PN molar ratio 100, NDA / KCN = 1, 0.025 mM [Fe(III)(CN)₆]³⁻ / 0.05 mM [Fe(II)(CN)₆]⁴⁻ molar ratio 0.5 in buffer 100 mM borate pH 9 / MeOH (50/50 v / v). Scan rate 25 mV s⁻¹ modulation time 100 ms modulation amplitude 7.5 mV under a flow rate of 0.05 μL.s⁻¹.

A detection limit of 25 nM in the microfluidic chip was obtained for a current of 10 pA. This detection limit was 10-fold less than that obtained in macrosystem with a traditional three-electrode set-up^[25] and over 100-fold less than that obtained with CE-LIF detection.^[27] Moreover, the stability of the detection signal with the used protocol is similar to the one found in conventional system of 3-electrodes where we found of lost a 20% (signal intensity) after 24 hours while no signal is detectable using an optical detection under the same storage conditions. The detection limit was 25 nM labelled peptide while reproducibility and sensitivity are equal to 5% and 1.36×10^{-10} A.μM⁻¹ by considering the three pairs of electrode per channel and similar for inter-device, respectively. For comparison, the detection limit of the labelled glycine with the NDA was determined by Yassine *et al.*^[31] in PDMS/Glass microfluidic chip with LIF detection at 40 nM with good reproducibility and a standard deviation of 1 to 2% was obtained for the peak intensity. Wang *et al.*^[32] have obtained a detection limit of 3.2 μM for labelled arginine and 7.4 μM and 3.5 μM for labelled phenylalanine and labelled glycine with amperometric detection in a microfluidic chip, respectively. They indicated detection with a good reproducibility through the obtained standard deviation between 3.1 and 3.5%. To conclude, our presented methodology is equally suitable for fast labelling and detection with similar sensitivity and reproducibility.

Conclusions

Previous works have demonstrated the feasibility of monitoring voltammetric waves using flow-channel electrode^{[14],[25]} or interdigitated microelectrodes array strategy with two-electrode set-up.^{[22],[23]} However, this present study with the associated detection scheme highlights an original two-microelectrode system for chip multi-use in the detection of ultralow concentration of peptide using a well-tested optical label. The

experimental results underline the analytical performance of this alternative with very good reproducibility and negligible variation of the signal without the need to implement a third electrode as reference. As portrayed the threshold of detection is in the nanomolar concentration range. Advantages of this configuration can be extended in many analytical or bioanalytical fields as end-column detectors in electrophoretic or chromatographic separation in miniaturized chips.

10 Acknowledgements

This research was supported by the French ANR (Agence Nationale de la Recherche) in the context of the P2N "DIMIPOLE" project.

Notes and references

¹⁵ ^a CNRS, UMR 8235, LISE, F-75005, Paris, France

* Jean.gamby@upmc.fr

^b Sorbonne Universités, UPMC Univ Paris 06, UMR 8235, Laboratoire Interfaces et Systèmes Electrochimiques, F-75005, Paris, France

^c CNRS, Institut Galien Paris-Sud, UMR 8612, F-92290 Châtenay-

²⁰ Malabry, France

^d Univ Paris-Sud, Faculté de Pharmacie, F-92290 Châtenay-Malabry, France

^e CNRS, Laboratoire de Photonique et de Nanostructures, UPR20, Marcoussis 91460, France

²⁵

[1] J. C. Sanders, Z. Huang and J. P. Landers, *Lab on a Chip* **2001**, *1*, 167-172.

[2] P. A. Limbach and Z. Meng, *Analyst* **2002**, *127*, 693-700.

[3] Z. Wu, H. Jensen, J. Gamby, X. Bai and H. H. Girault, *Lab on a Chip* **2004**, *4*, 512-515.

[4] C. F. Duffy, B. MacCraith, D. Diamond, R. O'Kennedy and E. A. Arriaga, *Lab on a Chip* **2006**, *6*, 1007-1011.

[5] T. C. Rohner, J. S. Rossier and H. H. Girault, *Analytical Chemistry* **2001**, *73*, 5353-5357.

³⁵ [6] S. Le Gac and A. van den Berg in *Chapter 1 Introduction*, Vol. The Royal Society of Chemistry, **2009**, pp. 1-20.

[7] Y. Liu, H. Wang, Q. Liu, H. Qu, B. Liu and P. Yang, *Lab on a Chip* **2010**, *10*, 2887-2893.

[8] M. Abonnenc, L. Dayon, B. Perruche, N. Lion and H. H. Girault, *Analytical Chemistry* **2008**, *80*, 3372-3378.

[9] D. W. M. Arrigan, *Analyst* **2004**, *129*, 1157-1165.

[10] C. Amatore, C. Sella and L. Thouin, *J. Electroanal. Chem.* **2006**, *593*, 194-202.

[11] S. Méance, K. Papin, J. Gamby, G. Aubry, Q. Kou and A.-M. Haghiri-Gosnet, *Microelectronic Engineering* **2011**, *88*, 1798-1800.

[12] X.-S. Zhou and E. Maisonhaute, *Electrochemistry (Cambridge, U. K.)* **2013**, *11*, 1-33.

[13] M. Kechadi, J. Gamby, L. Chaal, H. Girault, B. Saidani and B. Tribollet, *Electrochimica Acta* **2013**, *105*, 7-14.

⁵⁰ [14] R. G. Compton, A. C. Fisher, R. G. Wellington, P. J. Dobson and P. A. Leigh, *J. Phys. Chem.* **1993**, *97*, 10410-10415.

[15] K. Stulik, C. Amatore, K. Holub, V. Marecek and W. Kutner, *Pure Appl. Chem.* **2000**, *72*, 1483-1492.

[16] N. V. Rees, O. V. Klymenko, E. Maisonhaute, B. A. Coles and R. G. Compton, *J. Electroanal. Chem.* **2003**, *542*, 23-32.

[17] J. S. Rossier, M. A. Roberts, R. Ferrigno and H. H. Girault, *Analytical Chemistry* **1999**, *71*, 4294-4299.

[18] I. Streeter, N. Fietkau, J. Del Campo, R. Mas, F. X. Munoz and R. G. Compton, *J. Phys. Chem. C* **2007**, *111*, 12058-12066.

⁶⁰ [19] O. Ordeig, N. Godino, J. del Campo, F. X. Muñoz, F. Nikolajeff and L. Nyholm, *Analytical Chemistry* **2008**, *80*, 3622-3632.

[20] B. J. Polk, A. Stelzenmuller, G. Mijares, W. MacCrehan and M. Gaitan, *Sens. Actuators, B* **2006**, *114*, 239-247.

[21] J. Zhou, K. Ren, Y. Zheng, J. Su, Y. Zhao, D. Ryan and H. Wu, *Electrophoresis* **2010**, *31*, 3083-3089.

[22] V. N. Goral, N. V. Zaytseva and A. J. Baeumner, *Lab on a Chip* **2006**, *6*, 414-421.

[23] S. Kwakye, V. N. Goral and A. J. Baeumner, *Biosensors and Bioelectronics* **2006**, *21*, 2217-2223.

⁷⁰ [24] M. Lazerges, V. T. Tal, P. Bigey, D. Scherman and F. Bedioui, *Sensors and Actuators B: Chemical* **2013**, *182*, 510-513.

[25] M. Faure, S. Korchane, I. Le Potier, A. Pallandre, C. Deslouis, A.-M. Haghiri-Gosnet and J. Gamby, *Talanta* **2013**, *116*, 8-13.

[26] T. Hu, H. Zuo, C. M. Riley, J. F. Stobaugh and S. M. Lunte, *J. Chromatogr. A* **1995**, *716*, 381-388.

[27] S. Korchane, A. Pallandre, C. Przybylski, C. Poas, F. Gonnet, M. Taverna, R. Daniel and I. Le Potier, *Electrophoresis* **2014**, *35*, 1050-1059.

[28] V. G. Levich, *Physicochemical Hydrodynamics*, Prentice-Hall, **1962**, p. 700 pp.

⁸⁰ [29] A. D. Clegg, N. V. Rees, O. V. Klymenko, B. A. Coles and R. G. Compton, *Journal of the American Chemical Society* **2004**, *126*, 6185-6192.

[30] C. Amatore, C. Pebay, L. Thouin and A. Wang, *Electrochem. Commun.* **2009**, *11*, 1269-1272.

⁸⁵ [31] O. Yassine, P. Morin, O. Dispagne, L. Renaud, L. Denoroy, P. Kleimann, K. Faure, J. L. Rocca, N. Ouaini and R. Ferrigno, *Analytica Chimica Acta* **2008**, *609*, 215-222.

[32] J. Wang, G. Chen and M. Pumera, *Electroanalysis* **2003**, *15*, 862-865.

⁹⁰